Asymptotic Behavior of Inflated Lattice Polygons

Mithun K. Mitra · Gautam I. Menon · R. Rajesh

Abstract We study the inflated phase of two dimensional lattice polygons with fixed perimeter N and variable area, associating a weight $\exp[pA - Jb]$ to a polygon with area A and b bends. For convex and column-convex polygons, we calculate the average area for positive values of the pressure. For large pressures, the area has the asymptotic behaviour $\langle A \rangle / A_{\max} = 1 - K(J)/\tilde{p}^2 + \mathcal{O}(\rho^{-\tilde{p}})$, where $\tilde{p} = pN \gg 1$, and $\rho < 1$. The constant $K(J)$ is found to be the same for both types of polygons. We argue that self-avoiding polygons should exhibit the same asymptotic behavior. For self-avoiding polygons, our predictions are in good agreement with exact enumeration data for $J = 0$ and Monte Carlo simulations for $J \neq 0$. We also study polygons where self-intersections are allowed, verifying numerically that the asymptotic behavior described above continues to hold.

Keywords Lattice polygons · Vesicles · Exact enumeration · Wulff construction

1 Introduction

The study of lattice polygons weighted by area and perimeter is a central problem in lattice statistics and combinatorics. Lattice polygons have been used to model vesicles [6, 11], cell membranes [22], emulsions [23], polymers [16] and percolation clusters [17]. In several cases, exact generating functions for classes of such polygons have been obtained. A survey of different kinds of lattice polygons and a review of related results can be found in [3, 24].

In this paper, we study the asymptotic behaviour of the area enclosed by inflated polygons of fixed perimeter. We calculate the area for two special cases of lattice polygons—convex

M.K. Mitra (✉) · G.I. Menon · R. Rajesh
The Institute of Mathematical Sciences, C.I.T. Campus, Taramani, Chennai 600113, India
e-mail: mithun@imsc.res.in

G.I. Menon
e-mail: menon@imsc.res.in

R. Rajesh
e-mail: rrajesh@imsc.res.in

and column-convex lattice polygons. We then conjecture the appropriate form for the area of self-avoiding polygons in the inflated phase.

We first summarize known results for the problem of pressurized polygons, based on the generating function

$$G(\mu, p) = \sum_{A,N} C_N(A) e^{pA} \mu^N, \tag{1}$$

where $C_N(A)$ is the number of self-avoiding polygons of perimeter N and area A, weighted by a chemical potential μ. Here p is the pressure which couples to the area A. Exact solutions exist for $G(\mu, p)$ when $C_N(A)$ is restricted to convex polygons [1, 2, 12] or to column-convex polygons [4]. However, a general solution for self-avoiding polygons is unavailable. Exact enumeration results for self-avoiding polygons exist for all N up to $N = 90$ and for all A for these values of N [10]. A transition at $p = 0$ separates a branched polymer phase when $p < 0$ (for μ sufficiently small) from an inflated phase when $p > 0$. At $p = 0$, the problem reduces to that of the enumeration of self-avoiding polygons. The scaling function describing the scaling behavior (for $p < 0$) near the tricritical point $p = 0$ and $\mu = \kappa^{-1}$, where κ is the growth constant for self-avoiding polygons, is also known exactly [5, 18, 19].

Less is known about the inflated phase obtained for positive pressures $p > 0$. However, this phase is of physical interest in the case of two-dimensional vesicles, or equivalently pressurized ring polymers [7, 8, 11, 14, 21]. In the calculations described in this paper, we consider the partition function

$$\mathcal{Z}_N(p, J) = \sum_{A,b} C_N(A, b) e^{pA - Jb}, \quad p > 0, \tag{2}$$

where $C_N(A, b)$ is the number of self-avoiding polygons of area A with b bends. A bending energy cost J per bend is introduced to incorporate semi-flexibility.

Some rigorous results exist for $\mathcal{Z}_N(p, 0)$ when $p > 0$. Reference [15] proved that

$$\mathcal{Z}_N(p, 0) = A(p) e^{pN^2/16} (1 + \mathcal{O}(\rho^N)) \quad \text{as } N \to \infty, \tag{3}$$

for some $0 < \rho < 1$, with $A(p)$ some function of p. This result holds in the limit where $N \to \infty$ keeping p fixed. However, as we argue in Sect. 2, the relevant scaling limit in the inflated regime is $p \to 0$, $N \to \infty$ keeping $\tilde{p} = pN$ finite.

The central results of the paper are the following: We calculate expressions for the area for convex (see (19)) and column-convex (see (31), (35) and (37)) polygons. In the limit $\tilde{p} \gg 1$, we show that for both convex and column-convex polygons, the area is given by,

$$\langle A \rangle = \frac{N^2}{16} \left[1 - \frac{32\pi^2}{3\tilde{p}^2} + \frac{64}{\tilde{p}^2} \text{Li}_2 (1 - \alpha) \right] + \mathcal{O}(e^{-\tilde{p}/8}), \tag{4}$$
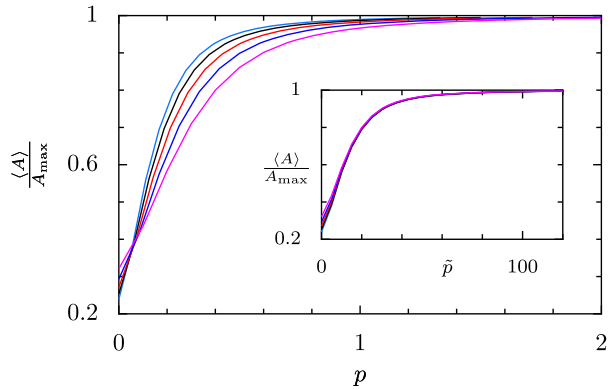
where Li_2 is the dilogarithm function

$$\text{Li}_2(x) = \sum_{m=1}^{\infty} \frac{x^m}{m^2}, \tag{5}$$

and, $\alpha = e^{-2J}$. We argue that this result should also extend to the self-avoiding case and test this conjecture numerically.

The paper is organized as follows. In Sect. 2, we present a justification of the scaling limit we consider using a simply scaling argument. Sections 3 and 4 contain the calculation of the

area for convex and column-convex polygons respectively. Section 5 contains the numerical
analysis of self-avoiding polygons and self intersecting polygons. A brief summary of our
results and conclusions is presented in Sect. 6.

2 Scaling in the Inflated Regime

The inflated regime of self-intersecting pressurized polygons has been well studied in the
continuum [7, 8, 14, 21]. In this case the appropriate scaling variable is obtained by scaling
the thermodynamic pressure with the system size, taking $p \to 0$, $N \to \infty$ keeping $\tilde{p} = pN$
finite. A typical configuration in the inflated phase has no self-intersections. Thus, we expect
that the above scaling should also hold for self-avoiding polygons.

This choice of the scaling variable can be motivated by simple scaling arguments. The
pressure contribution to the free energy in the inflated phase is given by

$$F = -pA \approx -pR^2 \approx -pN^2, \tag{6}$$

since $\langle R \rangle \sim N$ in this regime. However, the free energy of a polygon of perimeter N, being
an extensive variable, scales linearly with N. In order to make these two energies compara-
ble, the pressure should scale inversely with N, i.e. $p \sim 1/N$.

In Fig. 1, we show the variation of $\langle A \rangle / A_{\max}$ with pressure p, where $A_{\max} = N^2/16$ is
the maximum possible area. The data points collapse onto one curve when p is scaled as
$\tilde{p} = pN$. The data is obtained from exact enumerations of self-avoiding polygons on the
square lattice [9].

3 Convex Polygons

In this section we calculate the equilibrium shape and area of a convex polygon when $\tilde{p} > 0$.
Convex polygons are those polygons which have exactly 0 or 2 intersections with any ver-
tical or horizontal line drawn through the midpoints of the edges of the lattice (see Fig. 2).
We calculate the area by determining the shape of the convex polygon that minimizes the
free energy at fixed perimeter, generalizing the calculation presented in [17].

The perimeter N of a convex polygon is the same as that of its bounding box, which, in
general, is a rectangle. The equilibrium shape should however be invariant about rotations

Fig. 2 (Color online)
A schematic diagram of a convex
polygon. Any vertical or
horizontal line (thick *dashed
lines*) intersects the convex
polygon at either 0 or 2 points
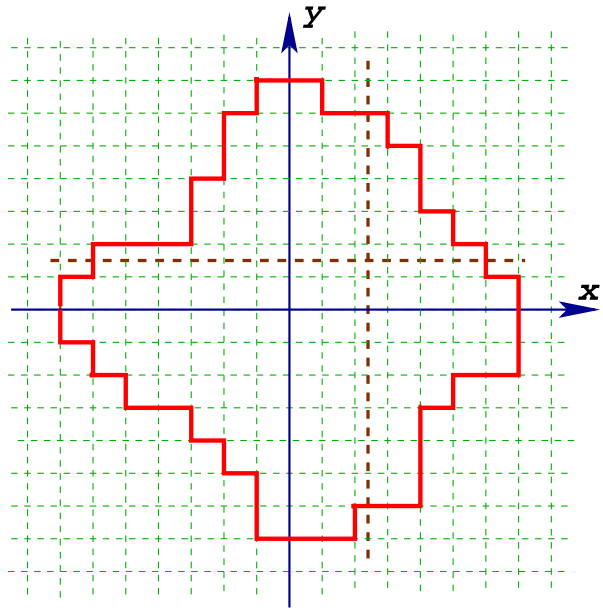
by angle $\pi/2$. The bounding box of the equilibrium shape is thus a square of side $N/4$. We can now calculate the shape in the first quadrant, obtaining the shapes in other quadrants by symmetry.

Consider a coarse grained shape $y(x)$ in the first quadrant with endpoints at $(0, N/8)$ and $(N/8, 0)$. The free energy functional for this curve $y(x)$ can be written as

$$\mathcal{L}[y(x)] = \int_0^{N/8} dx\, \sigma(y')\sqrt{1 + y'^2} - \frac{\tilde{p}}{N} \int_0^{N/8} dx\, y, \tag{7}$$

where $\sigma(y')$ is the free energy per unit length associated with a slope y' and $\tilde{p}$ is the scaled pressure. The shape is then obtained from (7) through the Euler Lagrange equation (Wulff construction) [20],

$$\frac{d}{dx} \frac{d}{dy'} \left[\sigma(y')\sqrt{1 + y'^2} \right] = -\frac{\tilde{p}}{N}. \tag{8}$$

The free energy can be calculated using a simple combinatorial argument. Consider all possible paths starting from $(0, y)$ and ending at $(x, 0)$ with only rightward and downward steps. The weight of a path is $\exp(-Jb)$, where b is the number of bends. When $x, y \gg 1$, the weighted sum of these paths will be equal to $\exp[-\sqrt{x^2 + y^2}\sigma(y')]$, where y' is the mean slope of the path.

Let $C(x, y)$ be the sum of weighted walks constructed as above. Such walks may be enumerated by splitting the path into sequences of rightward and downward steps and associating the bending energy term to a sequence of downward (y) steps begun and terminated by a step to the right. Then

$$C(x, y) = \sum_{y_1, y_2, \ldots, y_X} \prod_i W_i\, \delta\left[\sum y_i - y\right], \tag{9}$$

where W_i is the weight associated with the ith step, which is given by

$$W_i = [\alpha(1 - \delta_{y_i,0}) + \delta_{y_i,0}], \tag{10}$$

and $\alpha = e^{-2J}$. The delta function enforces the constraint that the steps taken in the y-direction must total y. The summation is over all possible numbers of steps taken in the y direction at steps $1, 2, \ldots, x$.

Performing a discrete Laplace transform, we obtain

$$\sum_y C(x, y)\omega^y \approx \left[1 + \alpha\omega + \alpha\omega^2 + \cdots\right]^x$$

$$= \left[\frac{1 - (1 - \alpha)\omega}{1 - \omega}\right]^x. \tag{11}$$

For large x, y, the inverse Laplace transform can be calculated using the saddle point approximation. This gives

$$\sigma(y') = \frac{-f(\omega^*)}{\sqrt{1 + y'^2}}, \tag{12}$$

where

$$f(\omega) = y' \ln(\omega) + \ln[1 - (1 - \alpha)\omega] - \ln(1 - \omega), \tag{13}$$

and ω^* satisfies

$$\left.\frac{df}{d\omega}\right|_{\omega^*} = 0. \tag{14}$$

The equilibrium shape can now be obtained from (8) and (12). The shape satisfies the equation

$$ce^{\tilde{p}X} + cc_1 e^{\tilde{p}(X+Y)}(1 - \alpha) - c_1 e^{\tilde{p}Y} = 1, \tag{15}$$

where X and Y are scaled coordinates defined as $X = x/N$ and $Y = y/N$. The constants of integration are fixed by imposing the requirement that the shape should be symmetric under the interchange of X and Y, and the boundary condition that $y(x = N/8) = 0$. This gives,

$$c = -c_1 = \frac{(1 + e^{-\tilde{p}/8}) - \sqrt{(1 + e^{-\tilde{p}/8})^2 - 4e^{-\tilde{p}/8}(1 - \alpha)}}{2(1 - \alpha)}, \tag{16}$$

and the equilibrium shape can be written as

$$ce^{\tilde{p}X} - c^2 e^{\tilde{p}(X+Y)}(1 - \alpha) + ce^{\tilde{p}Y} = 1. \tag{17}$$

The shapes for different values of the scaled pressure are shown in Fig. 3 for a convex polygon with $J = 1$.

The area of the convex polygon is obtained from the equilibrium shape as

$$\langle A \rangle = 4N^2 \int_0^{1/8} Y \, dX, \tag{18}$$

Fig. 3 (Color online) Shape of
the convex polygon as obtained
from (17) for polygons with
$J = 1$. The different shapes
correspond to pressure values
$\tilde{p} = 1.0, 10.0, 50.0$, with the
outer shape corresponding to
largest pressure
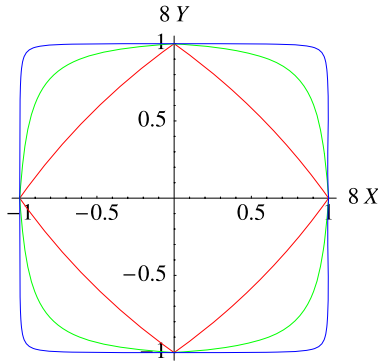
where the factor of 4 corresponds to the four quadrants. Doing the integration, we obtain

$$\langle A \rangle = \frac{N^2}{16} \left[-\frac{8 \ln(c)}{\tilde{p}} + \frac{64}{\tilde{p}^2} \left(\mathrm{Li}_2[c] - \mathrm{Li}_2[c \ e^{\tilde{p}/8}] \right. \right.$$
$$\left. \left. + \mathrm{Li}_2[c(1 - \alpha)e^{\tilde{p}/8}] - \mathrm{Li}_2[c(1 - \alpha)] \right) \right], \tag{19}$$

where Li_2 is the dilogarithm function.

The asymptotic behavior for large $\tilde{p}$ may be calculated from (16) and (19). When $\tilde{p} \gg 1$, the constant c can be written as,

$$c = e^{-\tilde{p}/8} + \mathcal{O}(e^{-\tilde{p}/4}). \tag{20}$$

Substituting into (19), we obtain

$$\langle A \rangle = \frac{N^2}{16} \left[1 - \frac{32\pi^2}{3\tilde{p}^2} + \frac{64}{\tilde{p}^2} \mathrm{Li}_2(1 - \alpha) \right] + \mathcal{O}(e^{-\tilde{p}/8}). \tag{21}$$

When $J = 0$, the last term on the right hand side of (21) is zero and the relation reduces to

$$\langle A \rangle = \frac{N^2}{16} \left[1 - \frac{32\pi^2}{3\tilde{p}^2} \right] + \mathcal{O}(e^{-\tilde{p}/8}), \qquad J = 0. \tag{22}$$

4 Column-Convex Polygons

In this section, we calculate the shape and area of a column-convex polygon when $\tilde{p} > 0$. Column-convex polygons are those polygons which have exactly 0 or 2 intersections with any vertical line drawn through the midpoints of the edges of the lattice. There, is however, no such restriction in the horizontal direction (see Fig. 4). We calculate the area by determining the shape of the column-convex polygon that minimizes the free energy for a fixed perimeter.

The perimeter of a column-convex polygon has no simple relation to its bounding box. We thus introduce a chemical potential μ that couples to the perimeter N. Consider a shape $y(x)$ with endpoints at $(-\beta N, 0)$ and $(\beta N, 0)$. The free energy functional for this curve

Fig. 4 (Color online)
A schematic diagram of a
column-convex polygon. Any
vertical line intersects the convex
polygon at either 0 or 2 points
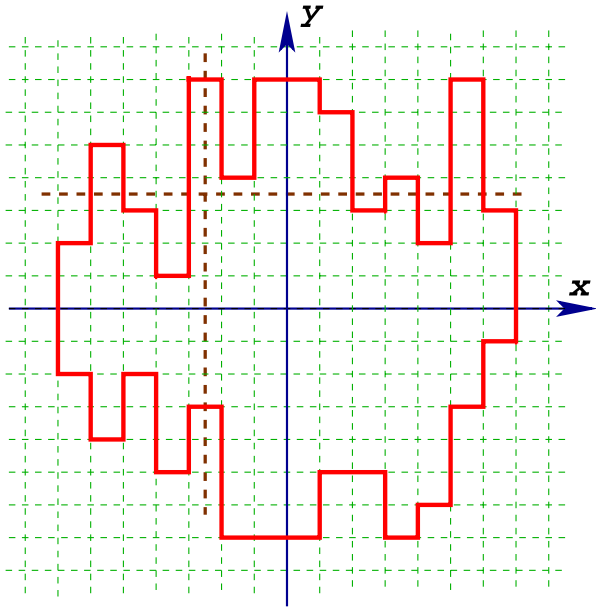
$y(x)$ is given by

$$\mathcal{L}[y(x)] = \int_{-\beta N}^{\beta N} dx\, \sigma(y')\sqrt{1 + y'^2} - \frac{\tilde{p}}{N}\int_{-\beta N}^{\beta N} dxy, \qquad (23)$$

where, $\tilde{p}$ is the scaled pressure, $\tilde{p} = pN$. As before, $\sigma(y')$ represents the free energy per
unit length associated with a slope y'. The Euler-Lagrange equation then gives the shape of
the equilibrium curve $y(x)$.

The free energy may be calculated as follows. Consider all paths starting from $(0,0)$ to
(x, y). Let $C(x, y)$ be the weighted sum of all paths. Then, we obtain

$$C(x, y) = \sum_{y_1, y_2, \ldots, y_X} \prod_i W_i\, \delta\left[\sum y_i - Y\right], \qquad (24)$$

where W_i is the weight associated with the ith step and equals

$$W_i = \mu^{|y_i|}\left[\alpha(1 - \delta_{y_i,0}) + \delta_{y_i,0}\right]\mu. \qquad (25)$$

Following the steps outlined previously, we convert the δ-function in (24) into an integral,
obtaining

$$C(x, y) = \frac{1}{2\pi}\int_0^{2\pi} ds e^{-isy}\left[f(\mu, \alpha, s)\mu\right]^x, \qquad (26)$$

where

$$f(\mu, \alpha, s) = \frac{1 + (1 - 2\alpha)\mu^2 + \mu(\alpha - 1)(e^{is} + e^{-is})}{(1 - \mu e^{is})(1 - \mu e^{-is})}. \qquad (27)$$

When $y \gg 1$, (26) may be evaluated by the saddle point method. Denoting y/x by y', we obtain

$$\sigma(y') = \frac{1}{\sqrt{1+y'^2}} \left[i s_0 y' - \ln \mu - \ln f(\mu, \alpha, s_0) \right], \tag{28}$$

where s_0 is the saddle point and is given by,

$$\frac{d}{ds_0} \ln f(\mu, \alpha, s_0) = i y'. \tag{29}$$

Substituting the expression for $\sigma(y')$ into the Euler-Lagrange equation (8) and using (29) we integrate once to obtain an equation for y'. This gives

$$y' = \frac{\mu(\alpha-1)(ce^{-\tilde{p}x/N} - c^{-1}e^{\tilde{p}x/N})}{1 + (1-2\alpha)\mu^2 + \mu(\alpha-1)(ce^{-\tilde{p}x/N} + c^{-1}e^{\tilde{p}x/N})}$$
$$+ \frac{\mu c e^{-\tilde{p}x/N}}{1 - \mu c e^{-\tilde{p}x/N}} - \frac{\mu c^{-1}e^{\tilde{p}x/N}}{1 - \mu c^{-1}e^{\tilde{p}x/N}}. \tag{30}$$

The constant of integration c is fixed by the condition that the slope of the equilibrium curve is 0 ($y' = 0$) at $x = 0$. This gives $c = 1$. Then we can integrate once more to obtain the equation of the equilibrium curve as

$$Y(X) = -\frac{c_1}{\tilde{p}} + \frac{1}{p} \ln \left[\frac{(1 - \mu e^{\tilde{p}X})(1 - \mu e^{-\tilde{p}X})}{1 + (1-\alpha)\mu^2 + \mu(\alpha-1)(e^{\tilde{p}X} + e^{-\tilde{p}X})} \right]. \tag{31}$$

As before, X and Y are defined as $X = x/N$ and $Y = y/N$. The constant of integration c_1 is fixed by the boundary condition $y(x = \beta N) = 0$. This gives,

$$c_1 = \ln \frac{(1 - \mu e^{\tilde{p}\beta})(1 - \mu e^{-\tilde{p}\beta})}{1 + (1-\alpha)\mu^2 + \mu(\alpha-1)(e^{\tilde{p}\beta} + e^{-\tilde{p}\beta})}. \tag{32}$$

The parameter β that determines the endpoint of the curve is still undetermined. It is chosen to be that β that minimizes the free energy. The Lagrangian $\mathcal{L}_0$ for this curve $Y(X)$ is given by substituting (31) and (32) into (23):

$$\mathcal{L}_0 = 2\beta N \int_0^1 dz \left[\ln \frac{(1 - \mu e^{\tilde{p}z\beta})(1 - \mu e^{-\tilde{p}z\beta})}{1 + (1-\alpha)\mu^2 + \mu(\alpha-1)(e^{\tilde{p}z\beta} + e^{-\tilde{p}z\beta})} - \ln \mu \right]. \tag{33}$$
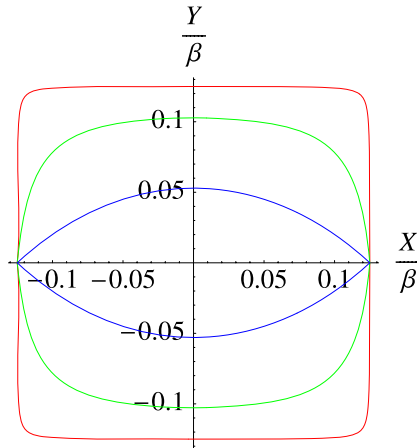
The parameter β satisfies the equation

$$\frac{d\mathcal{L}_0}{d\beta} = 0. \tag{34}$$

This gives

$$g(\mu, J) \equiv e^{\beta_0 \tilde{p}} = \frac{1 - \mu + \mu^2 - \mu^3(1-2\alpha)}{2\mu[1 + \mu(\alpha-1)]}$$
$$+ \frac{\sqrt{(1-\mu^2)[1 - 2\mu + \mu^2(1-2\alpha)][1 - \mu^2(1-2\alpha)]}}{2\mu[1 + \mu(\alpha-1)]}. \tag{35}$$

Fig. 5 (Color online) Shape of the column-convex polygon as obtained from (31) for polygons with $J = 1$. The different shapes correspond to pressure values $\tilde{p} = 3.0, 10.0, 50.0$, with the outer curve corresponding to the largest pressure. Both the X and Y axes are scaled by β

The chemical potential μ is determined by the constraint that total perimeter is N. This is equivalent to

$$\mu \frac{d\mathcal{L}_0}{d\mu} = -\frac{N}{2}. \tag{36}$$

μ then satisfies the equation,

$$-\frac{\tilde{p}}{4} = \ln \frac{1 - \mu g}{g - \mu} - \ln g + \frac{2 - a}{\sqrt{a^2 - b^2}} \ln \frac{(a+b)(g+1) + \sqrt{a^2 - b^2}(g-1)}{(a+b)(g+1) - \sqrt{a^2 - b^2}(g-1)}, \tag{37}$$

where a and b are given by

$$a = 1 + (1 - 2\alpha)\mu^2, \tag{38}$$

$$b = 2\mu(\alpha - 1). \tag{39}$$

This solves the equilibrium macroscopic shape completely. The shapes given by (31) are plotted in Fig. 5 for column-convex polygons with $J = 1.0$.

We now determine the asymptotic behavior of area when $\tilde{p} \gg 1$. This corresponds to the limit $\mu \to 0$. In this limit, $g(\mu, J)$ can be expanded as

$$g(\mu, J) = \frac{1}{\mu} - \alpha + \alpha(\alpha - 1)\mu - \alpha(\alpha - 1)^2\mu^2 + \mathcal{O}(\mu^3) \tag{40}$$

and (37) reduces to

$$\mu = e^{-\tilde{p}/8} + \mathcal{O}(e^{-\tilde{p}/4}). \tag{41}$$

Substituting the values of $g(\mu, J)$ and μ from (40) and (41) into (33), we can obtain the Lagrangian in the (μ, N) coordinates to be

$$\mathcal{L}_0(\mu, N) = \frac{\tilde{p}N}{32} + \frac{2N}{\tilde{p}}\left[\mathrm{Li}_2(1 - \alpha) - \frac{\pi^2}{6}\right] + \mathcal{O}(e^{-\tilde{p}/8}). \tag{42}$$

The Lagrangian in the $(\tilde{p}, N)$ coordinates can then be obtained by a Legendre transformation as

$$\mathcal{L}_0(\tilde{p}, N) = \mathcal{L}_0(\mu, N) + \ln(\mu)\frac{N}{2}, \tag{43}$$

$$= \frac{-\tilde{p}N}{32} + \frac{2N}{\tilde{p}}\left[\text{Li}_2(1-\alpha) - \frac{\pi^2}{6}\right] + \mathcal{O}(e^{-\tilde{p}/8}), \tag{44}$$

when $\tilde{p} \gg 1$. The area enclosed by the column-convex polygon is

$$A = -2N\frac{\partial\mathcal{L}_0}{\partial\tilde{p}}, \tag{45}$$

$$= \frac{N^2}{16}\left[1 - \frac{32\pi^2}{3\tilde{p}^2} + \frac{64}{\tilde{p}^2}\text{Li}_2(1-\alpha)\right] + \mathcal{O}(e^{-\tilde{p}/8}), \tag{46}$$

where the factor 2 in (45) accounts for the lower half plane. Interestingly, (46) is identical to (21) which is the asymptotic area expression for convex polygons.

5 Self-Avoiding and Self-Intersecting Polygons

In this section, we study the asymptotic behavior of self-avoiding and self-intersecting polygons. An analytic calculation along the lines of those presented for convex and column-convex polygons is not possible for self-avoiding polygons. However, we argue as follows: Convex polygons have no overhangs and the shape has four cusps. Introducing overhangs in one direction gives column convex polygons, reducing the number of cusps by two. Remarkably, the asymptotic behavior of the area in the column-convex case (equation (46)) coincides with that for convex polygons (equation (21)). It is therefore plausible that introducing overhangs in both directions does not affect the asymptotic behavior of the area, but merely removes the remaining two cusps, yielding a smooth shape. We therefore conjecture that the asymptotic behavior of the area of self-avoiding polygons is given by

$$\langle A \rangle = \frac{N^2}{16}\left[1 - \frac{32\pi^2}{3\tilde{p}^2} + \frac{64}{\tilde{p}^2}\text{Li}_2(1-\alpha)\right], \quad \tilde{p} \gg 1. \tag{47}$$

For self-intersecting polygons in the inflated phase, it is expected that the typical shape of the polygon does not intersect itself. Therefore, we argue that the area of self-intersecting polygons should also have the same asymptotic behavior as in (47).

These conjectures may be verified numerically. When $J = 0$, the area of self-avoiding polygons may be obtained using exact enumeration data on the square lattice [10]. This data is available for lengths up to $N = 90$ [9]. When $J \neq 0$, there is no exact enumeration data available. We therefore resort to Monte Carlo simulations. The Monte Carlo algorithm consists of a combination of global reflection and inversion moves [13]. The system size used was $N = 800$.

For self-intersecting polygons, the area may be computed using exact enumeration methods. We briefly describe the algorithm for the case $J = 0$. The generalization to non-zero J can be found in [14]. Consider a random walk starting from the origin and taking steps in one of the four possible directions. For each step in the positive (negative) x-direction, we assign a weight e^{-py} (e^{py}), where y is the ordinate of the walker. The weight is then e^{pA} for

Fig. 6 (Color online) The asymptotic behavior of the area for self-avoiding (SAP) and self-intersecting polygons (SIP). The *solid lines* correspond to the theoretical prediction of (47). The data is in good agreement with (47)
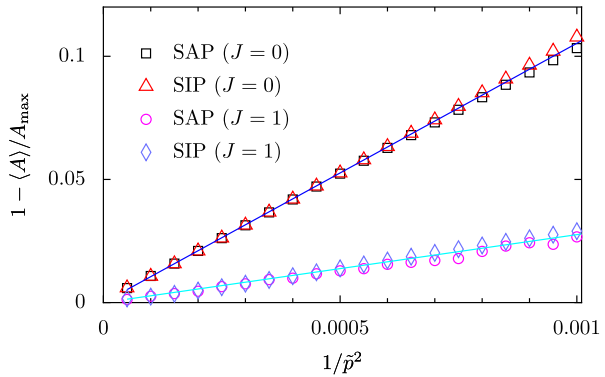
a closed walk enclosing an area A. Let $T_N(x, y)$ be the weighted sum of all N-step walks from $(0, 0)$ to (x, y). It obeys the recursion relation,

$$T_{N+1}(x, y) = e^{-py} T_N(x - 1, y) + e^{py} T_N(x + 1, y)$$
$$+ T_N(x, y - 1) + T_N(x, y + 1), \qquad (48)$$

with the initial condition

$$T_0(x, y) = \delta_{x,0}\delta_{y,0}. \qquad (49)$$

Finally, $T_N(0, 0)$ gives the partition function of the self-intersecting polygons on a lattice. We used exact enumeration data up to $N = 150$.

In the case of all exact enumeration data, for each pressure point, we extrapolated to $N \to \infty$ using finite size scaling. The results of the numerical analysis is shown in Fig. 6. The numerical data agree very well with the theoretical prediction.

6 Conclusions

We now summarize the basic results of this paper. For different types of polygons, we studied the dependence of area on pressure, in the inflated regime. For convex and column-convex polygons, we calculated the area using the Wulff construction. We found analytic expressions for these two classes of polygons for all positive values of $\tilde{p}$, where $\tilde{p} = pN$ in the limit $p \to 0$, $N \to \infty$, keeping pN fixed. The asymptotic behavior in the limit $\tilde{p} \gg 1$ was observed to coincide for both classes of polygons. We therefore conjectured that overhangs are not important in the inflated regime, and hence that self avoiding polygons should have the same asymptotic behavior. This was verified numerically. We also showed numerically that self intersections were irrelevant in the inflated regime. These results continue to remain valid in the presence of a non-zero bending rigidity.

Interestingly, the asymptotic behaviour for continuum ring polymers differs from that of lattice polygons. In the continuum, the analogous relation for the area of pressurized rings is asymptotically [8, 14]

$$\frac{\langle A \rangle}{A_{max}} \longrightarrow 1 - \frac{2\pi}{\tilde{p}}, \quad \tilde{p} \gg 1. \qquad (50)$$

This difference between continuum and lattice models is physically sensible in the expanded limit, since curvature in the lattice case is concentrated in local regions with $\pi/2$ bends but is delocalized along the contour in the continuum case.

While our conjectured result for self-avoiding polygons is in good agreement with numerical data, it would be of interest to have a mathematically rigorous derivation of this result. It may be possible to extend the methods of [15] to this problem.

References

1. Bousquet-Melou, M.: Convex polyominoes and algebraic languages. J. Phys. A **25**, 1935–1944 (1992)
2. Bousquet-Melou, M.: Convex polyominoes and heaps of segments. J. Phys. A **25**, 1925–1934 (1992)
3. Bousquet-Melou, M.: A method for the enumeration of various classes of column-convex polygons. Discrete Math. **154**, 1–25 (1996)
4. Brak, R., Guttmann, A.J.: Exact solution of the staircase and row-convex polygon perimeter and area generating function. J. Phys. A **23**, 4581–4588 (1990)
5. Cardy, J.: Exact scaling functions for self-avoiding loops and branched polymers. J. Phys. A **34**, L665–L672 (2001)
6. Fisher, M.E., Guttmann, A.J., Whittington, S.G.: Two-dimensional lattice vesciles and polygons. J. Phys. A **24**, 3095–3106 (1991)
7. Gaspari, G., Rudnick, J., Beldjenna, A.: The shapes and sizes of two-dimensional pressurized, self-intersecting rings, as models for two-dimensional vesicles. J. Phys. A **26**, 1–13 (1993)
8. Haleva, E., Diamant, H.: Smoothening transition of a two-dimensional pressurized polymer ring. Eur. Phys. J. E **19**, 461–469 (2006)
9. Jensen, I.: Number of sap of given perimeter and any area. http://www.ms.unimelb.edu.au/~iwan/polygons/series/sqsap_perim_area.ser
10. Jensen, I.: A parallel algorithm for the enumeration of self-avoiding polygons on the square lattice. J. Phys. A **36**, 5731–5745 (2003)
11. Leibler, S., Singh, R.R.P., Fisher, M.E.: Thermodynamic behaviour of two-dimensional vesicles. Phys. Rev. Lett. **59**, 1989–1992 (1987)
12. Lin, K.Y.: Exact solution of the convex polygon perimeter and area generating function. J. Phys. A **24**, 2411–2417 (1991)
13. Madras, N., Orlitsky, A., Shepp, L.A.: Monte Carlo generation of self-avoiding walks with fixed end-points and fixed length. J. Stat. Phys. **58**, 159–183 (1990)
14. Mitra, M.K., Menon, G.I., Rajesh, R.: Preprint. aXiv:0708.3318 (2007). To appear in Phys. Rev. E (2008)
15. Prellberg, T., Owczarek, A.L.: On the asymptotics of the finite-perimeter partition function of two-dimensional lattice vesicles. Commun. Math. Phys. **201**, 493–505 (1999)
16. Privman, V., Svrakic, N.: Directed Models of Polymers, Interfaces, and Clusters: Scaling and Finite-Size Properties. Springer, Berlin (1989)
17. Rajesh, R., Dhar, D.: Convex lattice polygons of fixed area with perimeter-dependant weights. Phys. Rev. E **71**, 016130 (2005)
18. Richard, C.: Scaling behaviour of two-dimensional polygon models. J. Stat. Phys. **108**, 459–493 (2002)
19. Richard, C., Guttmann, A.J., Jensen, I.: Scaling function and universal amplitude combinations for self-avoiding polygons. J. Phys. A **34**, L495–L501 (2001)
20. Rottman, C., Wortis, M.: Statistical mechanics of equilibrium crystal shapes: interfacial phase diagrams and phase transition. Phys. Rep. **103**, 59–79 (1984)
21. Rudnick, J., Gaspari, G.: The shapes and sizes of closed pressurized random walks. Science **252**, 422–424 (1991)
22. Satyanarayana, S.V.M., Baumgaertner, A.: Shape and motility of a model cell: A computational study. J. Chem. Phys. **121**, 4255–4265 (2004)
23. van Faassen, E.: Effects of surface fluctuations in a two-dimensional emulsion. Physica A **255**, 251–268 (1998)
24. van Rensburg, E.J.J.: The Statistical Mechanics of Interacting Walks, Polygons, Animals and Vesicles. Oxford University Press, Oxford (2000)